Editors' Suggestion

Design, integration, and commissioning of the first linac for image guided hadron therapy prototype

Alberto Degiovanni, Giovanni De Michele, Rossana Bonomi, Francisco Cabaleiro Magallanes, Michele Caldara, Veliko Dimov, Marco Esposito, Daniel Fink, Manuel Gallas Torreira, Yevgeniy Ivanisenko, Adam Jeff, Stefano Magnoni, Luis Navarro Quirante, Hannes Pavetits, Alessandra Valloni, Joël Adam, Debora Aguilera Murciano, Sandra Aumon, Carlo Baccigalupi, Laura Baiguera Tambutti, Sylvain Bailly, Sergio Ballestrero, François Bellorini, Stefano Benedetti, Alfonso Benot Morell, Denia Bouhired, Martin Breitenfeldt, Sylvain Candolfi, Giovanni Castorina, Matevz Cerv, Beatriz Conde Fernandez, Gerardo D'Auria, Cristovao Andre Dionisio Barreto, Luigi Salvatore Esposito, Adrian Fabich, Stefano Fanella, Daniel Fazio, Yoann Fusco, Francesco Galizzi, Stephen Gibson, Marina Giunta, Maria del Mar Gonzalez Fernandez, Paolo Gradassi, Alisa Healy, Vasim Khan, Lisa Kobzeva, Miguel Leal Seixas Correia, Gabriel Levy, Lucile Madoulaud, Guillaume Magrin, Antonio Marraffa, Claudio Mellace, Alberto Milla Moreno, Roland Moser, Diogo Murteira, Stephen Myers, Patricio Nadig, Jacopo Nardulli, Georg Nuessle, Yousri Ouerghi, Adriana Patino Revuelta, Pablo Paz Neira, Christopher Rejas, Diomedes Roman Concha, Theodore Rutter, Friederike Salveter, Alexandre Samochkine, Andres Sanchez Gonzalez, Dario Soriano Guillen, Pierpaolo Stabile, Katarzyna Stachyra, Donatella Ungaro, Bartlomiej Urbaniec, Margaux Vallé, Daniel Vazquez Rivera, Lionel Wallet, David Watts, and Carlo Zannini

AVO-ADAM, rue de Veyrot 11, CH-1217 Meyrin, Geneva, Switzerland

(Received 13 July 2023; revised 19 March 2024; accepted 4 April 2024; published 9 May 2024)

The Linac for Image Guided Hadron Therapy (LIGHT) system has been developed as the first commercial high-frequency linac-based proton therapy accelerator system. As part of the development process and of the technical validation of the concept, a reduced energy prototype linac (including all the key functional aspects of the full energy accelerator) has been designed and tested in parallel with the preparation work for a full-scale system. The LIGHT prototype construction, installation, and commissioning with beam allowed the identification of technical gaps and design improvements before the transfer to a medical device implementation. This paper gives a comprehensive summary of the design and integration aspects and presents for the first time the results achieved with the LIGHT prototype that was installed and commissioned on CERN premises in the years 2015–2019.

DOI: 10.1103/PhysRevAccelBeams.27.054701

I. INTRODUCTION

High-frequency hadron linacs for tumor therapy have been studied in the past decades to achieve the target energy of 230 MeV (for protons) and a beam current of few nA [1]. The Linac for Image Guided Hadron Therapy (LIGHT) is the heart of the beam production system of a linac-based proton therapy center. The LIGHT project, promoted by Applications of Detectors and Accelerators to Medicine, CERN spin-off (ADAM) started with the goal of building the LIGHT prototype at CERN (Conseil Européen pour la Recherche Nucléaire) premises to demonstrate its feasibility prior to the first "commercial" high-frequency linac-based solution for proton therapy.

At the beginning of the 90s, the concept of using medium-beta (energies ranging from 30 to 230 MeV) cell coupled linac (CCL) cavities with small bore hole apertures working at S-band frequencies (2.86 and 3 GHz) was introduced. For linear accelerators, the S-band frequency is well established since it is adopted for thousands of conventional x-ray therapy linacs [2]. From an industrialization point of view, this implies the direct commercial availability of radio frequency (rf) power sources and rf components, translating into less time to market. For the

low-energy part (up to 30–70 MeV), either a combination of radio-frequency quadrupole (RFQ) and drift tube linac (DTL) cavities or a low-energy cyclotron were considered [3,4].

The first proposals were followed by the construction and testing of a few prototype cavities and linac modules. The LIBO (LInac BOoster) module was designed, built, and tested with beam between 1998 and 2002, in a collaboration effort led by the Terapia con Radiazioni Adroniche Foundation together with CERN and the Istituto Nazionale di Fisica Nucleare (INFN) Sections of Milan and Naples. This accelerating unit was made of four "tanks," in which the average electric accelerating field was $E_0 = 16$ MV/m [5]. In the same years, other projects started and made progress on the design and prototyping of other types of high-frequency linac cavities for protons at low energy. A group from Energia Nucleare ed Energie Alternative (ENEA) in Frascati (Italy), within the Particle Accelerators and Medical Applications Laboratory, developed a novel side coupled drift tube linac (SCDTL) design for a proton linac project in Rome [6]. Following the experience with the LIBO module design, the group of INFN in Naples proposed a new design for CCL cavities and built a prototype for "A 3 GHz side Coupled LInac for Protontherapy" (ACLIP) project [7]. More recently, in 2013–2014, CERN made a novel design for a compact high-frequency RFQ that could be used as an injector of a 3 GHz proton linac [8].

The LIGHT system combines the 750 MHz RFQ built by CERN [8] with the low-beta side coupled drift tube linac (SCDTL) designed by ENEA [6] and the CCL adapted and redesigned by ADAM [9,10].

The LIGHT prototype was constructed and commissioned to energies up to 53 MeV, with the goal of demonstrating the feasibility of high-frequency linac technology for proton acceleration. Additionally, the development of a dedicated low-energy injection assembly (comprising the proton source and the low-energy beam transfer line) was fundamental to produce beams with properties adapted to proton therapy applications. Compared to previous experiences, for the first time, all the subsystems have been integrated into a fully operational machine used to accelerate proton beams, allowing to test key features of the LIGHT design (such as energy and intensity modulation, see Sec. V C) and to identify technical gaps and design improvements before its first medical implementation.

In this paper, a review of the design, installation, and operational aspects of the LIGHT prototype is reported. After an overview of the design specifications in Sec. II, a detailed description of the subsystems design is given in Sec. III. Important aspects related to the integration activities are described in Sec. IV. Finally, the beam commissioning process and the main measurement results are reported in Sec. V, which is followed by the conclusions in Sec. VI.

II. DESIGN SPECIFICATIONS

A. General linac design considerations

In the design of an accelerating structure, one of the main parameters to be considered is the effective shunt impedance. Such parameter is used to optimize the accelerating voltage and the power dissipated in a specific accelerating cell. Another important parameter is the peak surface field that a cavity can withstand. The above figures of merit will set the needed rf power for an accelerating cell for a given energy gain. The rf high-power source, whose choice is constrained by the technology used, by the operating frequency, or by economic reasons, can provide the rf peak power to the cavity to achieve the correct acceleration.

Given the available rf power, only a fixed number of cells can be fed by one high-power rf source. Furthermore, the increase in the particle's speed brings another constraint: each cavity length must be adapted to the speed of the particle and, since the speed is changing, the length of each cell shall also change. In reality, several cells with the same length can be grouped without losing efficiency, and more cells together make a so-called "tank." In general, the high-power rf source is chosen to feed at least one tank. Other factors, such as manufacturability, cost, flexibility, and modularity could play a role in the decision of the segmentation of the linac. For the LIGHT prototype, the decision was taken to have commercially available klystrons with a peak rf power of 7.5 MW (see Sec. III D). This available power was enough to feed several tanks (i.e., one or more rf modules, where one module is made by at least two tanks). Further to the consideration above, the linac design is driven by one of the key features and differentiators of LIGHT for proton therapy application: active energy modulation.

The distinction of the LIGHT active energy modulation system is the possibility to electronically change the power in the rf modules while being able to transport the beam along the linac. The choice of the number and gradients of the permanent magnet quadrupoles (PMQs), placed along the linac to create a fixed focusing-defocusing (FODO) lattice, is driven by this key feature.

B. The LIGHT prototype at point2

The first prototype of LIGHT has been adapted to be hosted on the CERN premises, as a demonstrator of the LIGHT system, where all main subsystems have been integrated.

As a demonstrator, the scope for the first prototype was limited to achieve the correct output beam energy, leaving out of scope considerations related to beam stability, beam emittance, and overall transmission optimization.

The maximum energy was limited to about 53 MeV due to the length of the available accelerator hall. This energy, although lower than the typical 230 MeV of clinical machines, was sufficient to validate the acceleration

TABLE I. Main linac parameters of the LIGHT prototype.

Module name	Q01	SM01	SM02	SM03	SM04	CM01	CM02
Structure type	RFQ	SCDTL	SCDTL	SCDTL	SCDTL	CCL	CCL
Number of tanks	Not applicable	11	13	9	7	2	2
rf frequency (MHz)	749.5	2997.9	2997.9	2997.9	2997.9	2997.9	2997.9
Cavities bore hole diameter (mm)	1.9–2.6	4.0	4.0	4.0	5.0	5.0	5.0
Effective shunt impedance (MΩ/m)	⋯	26	45	62	59	53/56	58/61
Peak surface electric field (MV/m)	51	54	84	76	79	99/98	95/94
Peak surface electric field (Kilp. Field)	2.02	1.15	1.8	1.6	1.7	2.1	2.03
Structure length (m)	2.00	1.12	1.70	1.52	1.60	0.80	0.83
Average accelerating field (MV/m)	68 kV[a]	11.1	16.2	16.5	16.0	16.5	16.5
Module rf peak power (MW)	0.40	0.83	2.59	2.46	2.48	2.21	2.21
Number of cavities per rf source	1/4[b]	2		1	1	2	
Number of PMQs	Not applicable	11	13	9	7	2	2
PMQs absolute gradients (T/m)	Not applicable	156–198	188–203	190	185	120–140	140
Output beam energy (MeV)	5.0	7.5	16.0	26.5	37.5	44.9	52.9

[a]Voltage across the RFQ vanes.
[b]Four IOTs are used to drive the RFQ.

process with all three types of LIGHT accelerating structures and to demonstrate the fast energy modulation capabilities of LIGHT (see Sec. V C). The prototype configuration included a proton source with a low-energy beam transfer (LEBT) line, the 750 MHz RFQ designed and built by CERN, four modules of SCDTL, and two modules of CCL. The main linac parameters of the LIGHT prototype are reported in Table I.

The LIGHT prototype was integrated into a concrete bunker (Fig. 1) within an existing hangarlike building at CERN (LHC-Point2 site). The building's internal layout had to be readapted and its services had to be refurbished, while others were fully designed and integrated from scratch (see Sec. II C). Figure 1 shows a three-dimensional (3D) model of the LIGHT prototype inside the bunker test area.

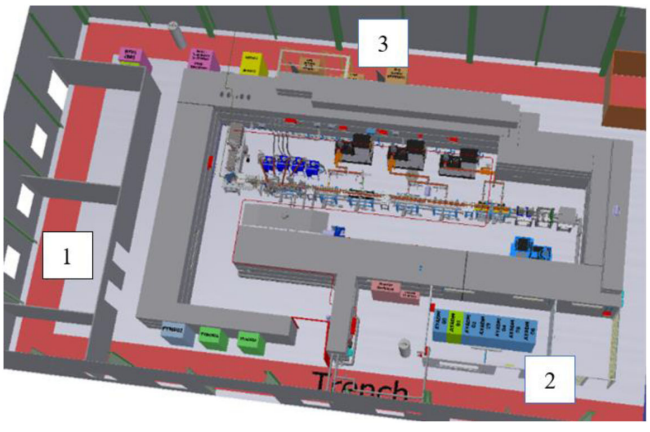

FIG. 1. Top view of the LIGHT prototype 3D model inside the bunker test area, with highlighted the main racks and areas: (1) Control room, (2) Rack room, (3) IOT Power System.

Given the building structure and available space, some compromises were made for the integration of the machine. Two important trade-offs were included: (1) the proton source and LEBT were fit in with a 90° bending angle (see Sec. III A) to leave more space for the accelerator; (2) the modulators and klystrons were installed inside the accelerator bunker.

C. Facility services

The bunker defining the radiation-controlled area inside the building was created with concrete and lead blocks while respecting the spatial limits given by the existing building services, trenches, and overhead crane. The bunker has an overall external maximum footprint of around 18×10 m^2 and an internal volume of around $16 \times 5 \times 2.2$ m^3 and is equipped with a maze access to protect against radiations.

An existing water-cooling system (based on a cooling tower) was refurbished and upgraded to distribute demineralized water to the dissipative components, such as rf network components, modulator-klystron systems (MKSs), inductive output tubes (IOTs), proton injector assembly (PIA), and beam diagnostics equipment inside the accelerator bunker (see Sec. III). Its water pump, driven by a speed drive motor and located externally to the building, provides demineralized water at 6 bar. The water was distributed into the bunker by a series of *ad hoc* stainless-steel manifolds equipped with manual regulating valves and flowmeters. A new water-cooling system (based on a

chiller) for the thermalization of the rf cavities was installed (see Sec. III F).

The Air Handling Unit of the building was recommissioned for ventilation purposes during the summer operation periods. An air-cooling system was designed and ordered according to the estimated heat loads generated inside the bunker (ca. 25 kW). The internal units have been installed inside the bunker, in suitable positions on the ceiling, in order to favor the fresh air circulation; the external unit has been installed outside the building; drainage has been directed toward the sewage inside the bunker. The accelerator bunker's nominal temperature has been set to 20 ± 1 °C.

A compressed air network, a steel pipe running on the bunker ceiling, provided 7 bar oil-free air to the pneumatic valves via a series of flexible hoses.

The total installed power for the prototype, when run at 200 Hz, was about 236 kW. The grounding copper bar of all beam line elements was derived from the main building earth terminal.

III. COMPONENTS DESIGN AND MANUFACTURING

In the design and manufacturing process, several technical challenges have been addressed. The integration of all the subsystem components into a functional system has highlighted design improvements that have been considered for the first LIGHT medical system. In this section, a review of the components' design and manufacturing is reported.

A. Source and LEBT

The proton source and the low-energy beam transfer (LEBT) line for the LIGHT prototype (Fig. 2) have been developed by Pantechnik [11], under the specifications from ADAM Source and LEBT together have been named LIGHT proton injector assembly (L-PIA).

The source is an electron cyclotron resonance ion source, providing a direct current (dc) proton beam up to 1 mA at 40 keV of energy. It is followed by a series of electrodes and electrostatic elements (Einzel lenses) that are used to achieve the beam intensity modulation (see Sec. V C) and to keep the beam focused up to the RFQ entrance. The LEBT also hosts a 90° dipole magnet, used to select the proton beam (with $Q/A = 1$) and disperse the unwanted H_2^+ ($Q/A = 1/2$) and H_3^+ ($Q/A = 1/3$) molecules extracted from the source. After the dipole magnet, a chopper with two electrode plates powered by an in-house designed pulsed power converter at about 16 kV allows to pulse the beam at a repetition rate of up to 200 Hz. When the electrodes are powered, the beam is deflected to an off-axis Faraday cup, where the beam current of the unchopped beam can be monitored. When no voltage is applied to the chopper, the beam continues straight along its path toward the RFQ.

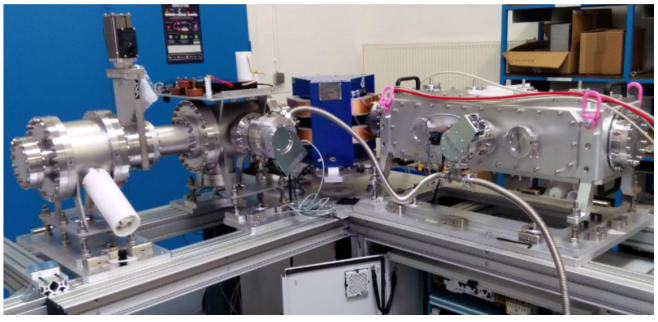

FIG. 2. The LEBT assembly of L-PIA for the LIGHT prototype.

B. RFQ injector at 750 MHz

The first accelerating stage, from 40 keV to 5 MeV, is achieved with a compact 750 MHz RFQ.

The design, made by CERN, was driven by the goal of making the most compact RFQ, allowing acceleration up to 5 MeV in only 2 m [8]. To achieve such a compact design, the nominal transmission efficiency of the beam was limited to about 30%, which was considered enough to match the core of the accelerated beam with the acceptance of the subsequent accelerating structures. Furthermore, the beam losses inside the RFQ are concentrated (by design) at energies below 1 MeV, which would not produce activation. The peak rf power needed is 399 kW, and it is generated by four commercial IOTs, made by Thales [12], used in pulsed mode. The IOTs are powered by a custom-designed power system, developed by CERN and installed outside the accelerator bunker, and based on a floating high voltage (HV) deck at −40 kV. The power is transported by coaxial lines and directly combined inside the RFQ (see Sec. III D).

The RFQ modules have been machined and brazed by CERN [13]. After the rf tuning [14], also performed at CERN, the RFQ was transported to the bunker test area to be installed in the beam line in February 2017 (see Sec. V A), as shown in Fig. 3.

FIG. 3. Installation of the radio frequency quadrupole of the LIGHT prototype in the bunker test area in 2017.

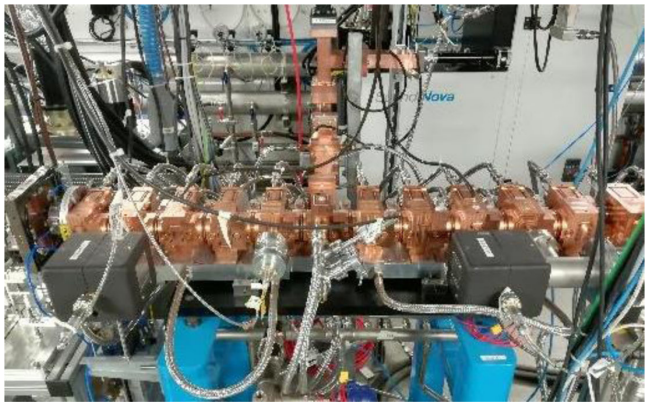

FIG. 4. The first SCDTL module of the LIGHT prototype.

C. High-frequency linac at 3 GHz

Downstream the RFQ, the next stages of LIGHT acceleration are achieved by two different types of structures: SCDTL up to 37.5 MeV, with 4 modules, and CCL up to 230 MeV, with 15 modules (2 modules to reach 53 MeV).

The SCDTL structures have been manufactured by T.S.C. [15]. The final assembly is achieved by two different technologies: vacuum brazing and tungsten inert gas (TIG) welding, also performed by T.S.C. The tuning was performed at the manufacturing company premises to achieve field flatness inside the tanks of better than 5%. The four modules of SCDTL (see Table I) for the LIGHT prototype were delivered in 2015–2016 and were installed in the beam line during 2017–2018 (see Sec. V A). A picture of SCDTL Module 1 (SM01) is shown in Fig. 4.

The CCL modules were designed in-house [10] and have been machined and vacuum brazed by VDL [16]. The main cells are machined as bricks and then brazed together to form tanks. Two tanks are connected via a "bridge coupler" that acts not only as a coupling element between the two tanks but also as the power coupler of the full module (see Fig. 5). The two CCL modules for the LIGHT prototype were delivered in 2017 and installed in the beam line in 2018 (see Sec. V A).

Between each rf tank, a PMQ was mounted around the beam pipes. The PMQ units are very compact, with a total length of 33 mm, and were produced by BJA [17]. The alignment of the rf modules and the PMQs was performed during the integration and installation stages with a dedicated laser tracker (see Sec. IV A).

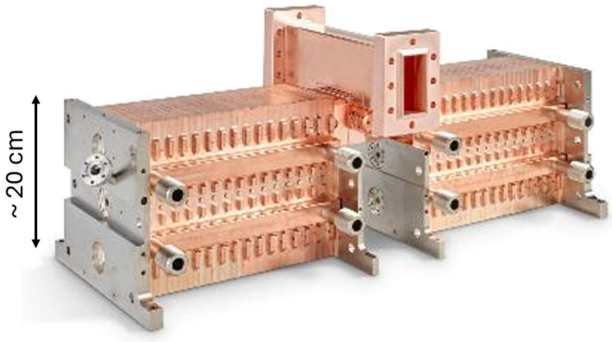

FIG. 5. Example of a CCL module after the final brazing.

D. High-power rf source and transport

The accelerating structures are fed with 750 MHz (RFQ) and 3 GHz (SCDTLs and CCLs) rf produced by specific high-power rf sources. The maximum average power required per unit goes from about 1 kW (for RFQ) to about 4 kW (for SCDTLs and CCLs). Two different power systems are used for the two frequencies.

The rf power system used for the RFQ consists of four IOTs (from Thales [12], model 795), used in pulsed mode at 749.48 MHz and powered by a custom-designed power system installed outside the accelerator bunker, based on a floating HV deck at −40 kV. The high-voltage power system for the IOTs has been designed and installed by CERN.

The 3 GHz structures are powered by pulsed klystrons (from Toshiba [18], model E3779), working at 2997.92 GHz, mounted on high-voltage pulsed split-core modulators (from Scandinova [19], model K1), generating up to 160 kV voltage pulses at the klystron gun with excellent pulse-to-pulse stability.

The rf power from the high-power stations to the accelerator modules is transported by the rf network (RFN) designed among others to preserve the rf quality. For the lower frequency, the network is made of four independent coaxial lines and the power handled does not exceed the 130 kW rf peak (500 W average) per line. For the 3 GHz sections, the RFN is made of rectangular waveguides and the maximum power handling corresponds to a peak rf power of 8 MW and an average rf power of 9 kW. The rectangular waveguide rf network (WR284) functions either in ultrahigh vacuum (UHV) conditions at an ultimate operating pressure of 10^{-7} mbar or under pressurized gas (SF_6). Some components also require cooling for thermal stabilization.

In terms of safety, the RFN follows the standard International Electrotechnical Commission (IEC) 60480:2019 standard to meet the European Union (EU) 517/2014 regulation.

The design is constrained by the maximum available rf power and the rf network insertion losses, hence its length shall take into consideration such constraints.

The rf network contains some components with key functionalities, including rf circulator/isolator, gas port, rf splitter, phase shifters, rf windows, and vacuum ports. Other components are also inserted, for diagnostics purposes and protection, such as bidirectional couplers, thermal sensors, thermal switches, and gas pressure gauges. Nonfunctional components, such as linear sections and/or bends, are also present to meet the specific installation site requirements (see Sec. II B). Other requirements are based

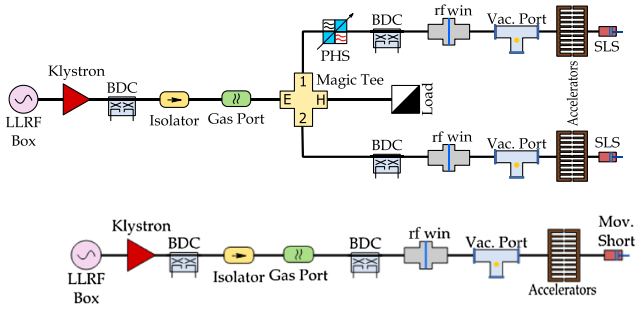

FIG. 6. Two possible configurations for the RFN of the 3 GHz section of the linac: two modules (top) and single module (bottom).

on performance and care was taken in the choice of the material, connections, flanges, and gaskets.

In the LIGHT prototype, the rf network had essentially two configurations: (i) feeding double-modules accelerating unit or (ii) feeding single-module accelerating unit (see Fig. 6). Both configurations were tested (as shown in Fig. 13). All rf networks and related components tested in the prototype performed as expected.

E. LLRF generation and synchronization

The overall machine rf field synchronization was ensured by a low-level rf (LLRF) system developed by Jim Potter Accelerator Works (JPAW) [20] and customized in a collaboration to fit the specific needs of the project. This system comprises a reference master oscillator (RMO) at 500 MHz, one LLRF unit at 750 MHz output to drive the RFQ, and three 3 GHz output LLRF units to drive two SCDTL units and a CCL unit. The LLRF units have measurement inputs for rf field from the cavities' pickups and from the rf network bidirectional couplers (Fig. 7).

The controls of the LLRF system allow independent control of phases and amplitudes of all units. There is an algorithm to close the phase loop through the cooling system controls.

The timing scheme is defined by the input trigger signal provided by the central timing system. It allows to shift the rf signal window with respect to the modulator high voltage timing window.

The LLRF system can generate rf arbitrary pulse shapes with up to 8-bit resolution in amplitude, and special shapes such as ramps-up and ramp-down. It is possible to modulate the output amplitude at 200 Hz. Feed forward

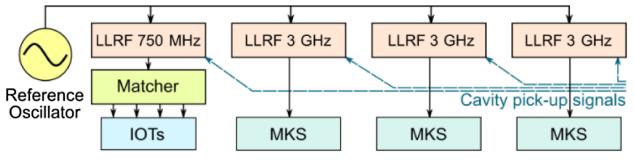

FIG. 7. LIGHT prototype LLRF system generic scheme.

phase and amplitude corrections are possible with the system but were not required to achieve the specifications.

The goal of the synchronization was to achieve a 1° root mean square (rms) phase jitter (at 3 GHz), with a stable phase delay between the units. The observed phase stability exhibited slow phase drifts, well correlated to the daily temperature cycle in the rack room. The phase stability of 1° rms was achieved.

F. Cooling system

All structures dissipate heat in the range of 1 to 5 kW thermal load in steady conditions and require a temperature stability in time of maximum 0.2 °C. This translated into careful thermal design of the embedded cooling circuits, as well as a bespoke cooling system solution based on water pumps and three-way regulating valves. The embedded circuits are either cooling channels drilled inside the copper walls of the cavities (RFQ and SCDTLs) or copper tubes directly brazed on the external surfaces (CCLs). Various considerations (e.g., temperature distribution, thermal expansion, cooling efficiency, erosion-corrosion) had to be considered during the design.

The chiller-based LIGHT cooling system can support up to 30 kW heat rejection and it includes different steps of regulating loops. It is compact and modular, such that the thermal parameters can be regulated for the single cavity. The chiller, main pumps, and controllers were in a bespoke barrack outside the building and were equipped with a condensation control system (which copes with freezing ambient temperatures), while the main components were integrated inside the bunker (along the walls) and on the supports of the cavities. Each module was equipped with a water circulator, three-way valve, and immersion temperature sensors. This same layout was reproduced 2 times upstream to achieve the desired modularity and stability.

To keep the thermal performance of each cavity stable, the system is based on a constant cooling flow, of which the supply temperature can be adjusted. The flow rates requested by the cavities are in the range of 30–60 l/ min per module, according to the type of module and nominal dissipated power. The water temperature stability can be obtained "manually" (selecting the adequate set point and PID control loop parameters of the valve) or via the LLRF regulation loop, which acts on the supply water temperature through the error feedback from the resonant frequency.

A less sophisticated water-cooling system, based on the existing CERN cooling tower, was also used for all the other LIGHT water-cooled components (see Sec. II C).

G. Vacuum system

The required base operating pressure of the LIGHT accelerator is in the 10^{-7} mbar region for the accelerating structures. To achieve this pressure, the system must fulfill

UHV requirements. It has been designed to be modular and it has been divided into several sectors, by sector valves.

The main vacuum components are pumps (turbomolecular, ion, and primary), pneumatic vacuum valves (sector and gate), manual service valves, vent valves, and penning gauges.

All the above components are off-the-shelf and were bought from Agilent [21] (pumping and pressure measurement) and VAT (valves) [22]. Further to these items, dedicated vacuum manifolds have been designed in-house to allow efficient pump-down and vacuum performance of each individual module. To validate the vacuum performance of components interfacing with the vacuum system [beampipes, beam diagnostic (BD) instruments, rf components, cavities, etc.], a vacuum test bench was built to perform leak detection, outgassing measurements, and residual gas analyzer analysis.

H. Control system and timing

The LIGHT Control System [23,24] has been developed by ADAM, with the objective of having a comprehensive yet simple monitoring and control of the accelerator subsystems. It consists of two parts, the supervisory control system (SCS) and the accelerator control system (ACS). The SCS provides non-real-time services and user interfaces. The ACS provides a unified interface to local control systems and equipment within the accelerator and beamline. Each device has a local front-end controller that interfaces the local control system to the user interfaces.

The slow control interface is a bidirectional software communication interface based on Siemens S7+ or OPCUA. WinCC-OA [25] is used as the Supervisory Control and Data Acquisition (SCADA) tool for non-real-time control and monitoring.

Software components have been developed in-house to allow the control of each single instrument (with user-level and expert-level interfaces), as well as the monitoring of the acquisition values during the time (as shown in Fig. 8). Moreover, a set of automated applications was available to run beam transverse profiles and emittance with different methods, Faraday cup and alternating current (ac) beam current transformer calibrations, 2D parameter scanning procedure, 200 Hz beam property measurements.

For the LIGHT prototype, the timing system used a trigger distribution box, having a time resolution of 10 ns and 80 ps rms jitter.

I. Machine and personnel safety system

The LIGHT-prototype machine and building have been equipped with interlock elements and control units that act as a machine and personnel safety system (MPSS).

The MPSS collects interlock signals from a number of subsystems/devices, and, upon evaluation of the internal interlock chains, it regenerates interlock signals for distribution to all connected subsystems/devices. The MPSS is designed as a slow-acting, robust system implemented in off-the-shelf hardware, prepared to comply with functional safety standards. The chosen platform is an SIEMENS PLC system of the SIEMENS SIMATIC S7-1500 series [26]. The MPSS houses digital input and digital output cards, as well as failsafe digital input and failsafe digital output cards.

A patrol safety system (PSS) was put in place to control the access to the radiation-controlled areas inside the facility, based on CERN rules.

An average current detector (ACD) was developed to monitor the average beam current accelerated out of the RFQ. For safety rule, the signal from the ACD was used to interlock the beam operation if the average beam current exceeded the value of 6 nA at the exit of the RFQ, which is the maximum allowed by the available radiation concrete shielding.

FIG. 8. Example of the in-house developed multiplot panel displaying acquisitions over time.

J. Beam diagnostics instruments

In order to commission the LIGHT prototype and to monitor the beam parameters, beam diagnostic instruments have been included in the design, as permanent elements. Particularly in the LEBT, as well as in two compact medium energy beam transport (MEBT) sections, the following fixed beam diagnostic devices were included (Table II): (i) A motorized slit and Faraday cup (FC), integrate into the so-called D-box, installed in the LEBT and used to measure beam profiles and beam current at low/medium energies (up to 37.5 MeV). (ii) Two beam position monitors (BPM), installed in the two MEBTs, used to measure the centroid beam position in x and y, and based on the use of capacitive pickups. (iii) Two ac beam current transformers (CT), installed in the two MEBTs, used to measure the macropulse beam current. (iv) A mini phase probe (PPR), installed along the SCDTL between SM02

TABLE II. Permanent diagnostics devices installed in the LIGHT prototype.

Category	Instrument	Measured parameter
Noninterceptive	ACCT	Intensity
	BPM	Centroid transverse position
	PPR	Bunch phase
	ToF	Beam energy
Interceptive	Slit + FC (DBox)	Beam profile, Intensity
	FSM	Beam profile
	FC, MLFC	Beam pulse charge, beam energy
	OPT + camera	Beam shape, beam position

and SM03, to monitor the beam-to-rf phase delay based on the use of capacitive pickups.

Additional diagnostic devices were also used temporarily as part of test benches installed during the different commissioning phases (see Sec. IV C). These included (i) three PPRs used to measure the beam energy, based on the time-of-flight (ToF) technique [27]; (ii) a fiber scanning monitor (FSM) used to measure the beam profile at energies above 30 MeV; (iii) a scintillating optical screen (OPT), with a charge-coupled device (CCD) camera, used as a simple and fast check of the beam position and shape; (iv) a Faraday cup and a multilayer Faraday cup (MLFC).

IV. INSTALLATION AND INTEGRATION

The installation and integration of the different subsystems happened in phases, corresponding to an increasing number of modules installed and output beam energy. At each phase, one or more modules were added to the beam line, and the beam was characterized by means of a movable diagnostic test bench. Before starting the beam commissioning of each phase, the new modules installed need to be conditioned at high power, aligned, and the beamline equipped with the appropriate vacuum and beam diagnostics instrumentation (fixed diagnostics and test benches).

A. Alignment

The LIGHT accelerator is quite demanding in terms of position accuracy and quite sensitive to alignment errors since it is composed of compact devices with small beam apertures. Therefore, the survey and position adjustment of its main beam line components are critical and have required a careful study of the most suitable and appropriate instrumentation and methodologies to be used from the early stages of design, with the aim of optimizing the process not only in terms of performance but also balancing the solutions adopted against practical and financial convenience.

The positional accuracy needed for each component has been estimated by performing beam dynamics studies and simulations, which have produced (as an outcome) the following needs for the most critical beam line components: (i) accelerating structures: 0.1 mm; (ii) permanent magnet quadrupoles (PMQ): 0.05 mm.

Beam diagnostic (BD) devices have less stringent requirements in terms of position accuracy; however, their position needs to be precisely measured and logged to allow for reliable measurement of beam properties.

The overall position uncertainty depends on several factors, the main ones being the precision of the survey, the accuracy in relating external visible geometry to internal structure geometry/fields, and the resolution and accuracy of position adjustment.

A reference network of nodes distributed within the prototype facility hall has been installed and precisely characterized before starting the installation of any of the LIGHT components. The network was made of approximately 20 points distributed along the beam line (on the right-hand and left-hand side walls, as well as on the low-energy side and high-energy side walls). The nodes have been installed at three different levels of height: one very low (about 20 cm above ground), one approximately at beam height (120 cm from floor level), and one high (at approximately 2 m height). A coordinate system has also been defined and related to the reference network to be used for survey and alignment operations, as well as for specifying the position of beam line components.

Using the reference network described above, the mechanical alignment of most critical LIGHT components has been performed by using a laser tracker [28]. This has been sufficient for aligning all components requiring a positional tolerance of 0.1 mm at the best (all LIGHT components except for PMQs) and for providing the "as installed" position of all BD detectors.

For the PMQs, in addition to a laser-tracker-based alignment, a solution allowing for fine position adjustment from a remote location has been developed. The latter has been done by designing a custom motion system using off-the-shelf miniature motors, adapted to control some mechanical actuators, through a custom-designed control system. This modified off-the-shelf solution has allowed to significantly reduce the cost of the system, still guaranteeing the performance and reliability of a fully

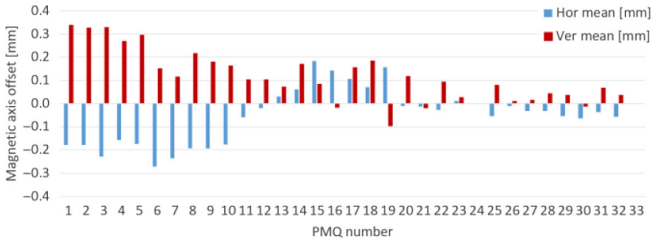

FIG. 9. Main results from PMQ test bench for the first 33 PMQs. The offset between the magnetic axis and mechanical axis shows an improvement between the first batch (up to PMQ 13) and the second batch (from PMQ 14 to PMQ 33).

commercial solution. This solution has provided the possibility to perform beam-based alignment with micrometric resolution.

LIGHT components required high-precision fiducialization to characterize the internal geometry and refer it to the designed external target points (fiducials). This has been done whenever possible during the manufacturing process by dimensional control of internal and external features using high-precision coordinate measuring machines (CMM).

Also in this case, the PMQs have represented an exception with respect to the "standard" procedure and have required a dedicated magnetic and mechanical characterization process.

PMQ magnetic characterization has been performed by means of a dedicated test bench using a vibrating wire [29]; this has allowed to perform a characterization of the magnetic field for each magnet as well as to relate the fiducials directly to the magnetic axis (Fig. 9).

In addition to this, given the very small dimensions of the PMQs (about 30 mm length and 15 mm outer diameter), there was no possibility of having fiducials directly on the PMQ body. Dedicated holes for targets were therefore incorporated in the mechanical supports and the characterization was performed with the PMQ already mounted on its "L-shaped support." A precision fit mating between PMQ and "L support" has been realized, however, to reduce even further the possibility of position uncertainty, the PMQs (after characterization) were installed on the beam line without being disconnected from their support.

B. rf conditioning of structures

rf cavities must undergo an rf conditioning process before they can achieve and sustain the nominal power for acceleration. The conditioning process smoothly raises the average power in the cavity, iterating in three parameters: rf peak power, pulse repetition rate, and rf pulse width. During the conditioning process, rf breakdowns occur. The ultimate goal of the conditioning is to achieve nominal power with a breakdown rate below the limits imposed for a successful treatment.

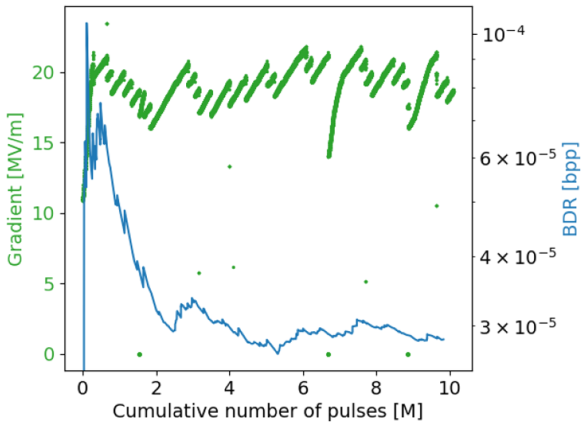

FIG. 10. Example of conditioning curve of a CCL module.

During the test periods of the LIGHT prototype, the conditioning process was developed and ultimately fully automatized by an in-house design, the so-called event detection system (EDS). The EDS contains all the necessary hardware and software to perform the conditioning of rf cavities with minimal human supervision [30]. The system is able to monitor key variables for the conditioning, detect breakdowns, and control rf power properties to successfully bring the cavity to nominal operation while keeping the breakdown rate within acceptable limits. Figure 10 depicts the critical part of the conditioning process of a CCL structure during EDS validation tests. After reaching nominal rf parameters, the EDS keeps the structure running rf until the breakdown rate goal is achieved.

C. Diagnostics test-benches

Beam diagnostic (BD) devices are essential to commission beams in a new accelerator. In addition, there is general experience indicating that fixed BD instrumentation systems installed in key locations along the accelerator are crucial to allow understanding and resolution of beam dynamics issues. Finally, BD devices allow the logging of important beam parameters during the machine Quality assurance (QA), thereby helping the identification of slow drifts or discrepancies from reference settings. In the LIGHT accelerator, the main BD challenges were to develop compact but sensitive instrumentation capable of following (in real time) the intensity and energy changes of the beam on a pulse-to-pulse basis. Several BD technologies were exploited so as to have a comprehensive set of tools allowing to fully characterize the beam during commissioning and a family of devices (mainly noninterceptive) installed in fixed positions along the accelerator (see Sec. III J), allowing beam monitoring in normal operation/treatment mode.

Three BD test benches have been designed and used during the different integration phases of the LIGHT

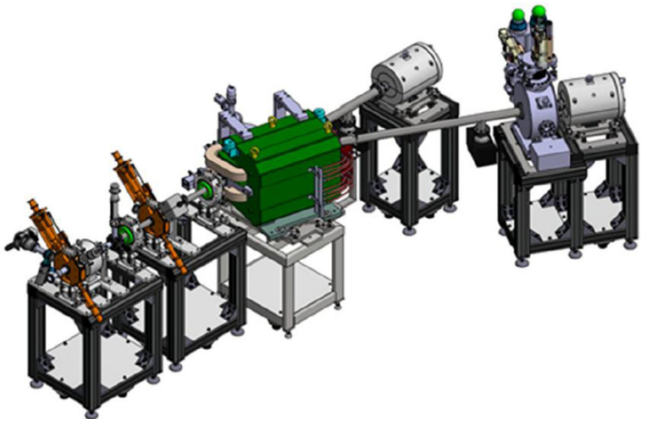

FIG. 11. 3D model of the medium energy test bench.

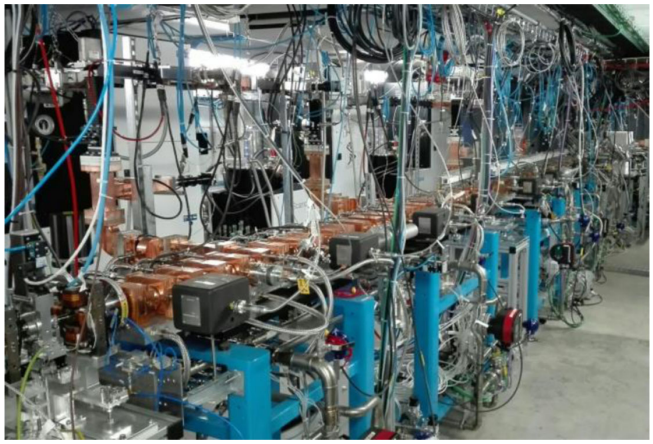

FIG. 12. View of the LIGHT prototype installed at CERN Point2 during the commissioning phase e. at 37.5 MeV.

prototype [31]: the low-energy (LE) test bench (at 40 keV), the medium-energy (ME) test bench (5–16.5 MeV), and the high-energy (HE) test bench (37.5–52 MeV).

Figure 11 displays the 3D model of the medium-energy test bench, which included several diagnostic elements, as well as two electromagnetic quadrupoles and one dipole used as a spectrometer magnet. In the test benches, the different BD devices were used in combination with the optics elements to perform complex beam optical parameters measurements (emittance reconstruction and energy spread) based on scans and applications, implemented in the control system.

V. BEAM COMMISSIONING AND BEAM CHARACTERIZATION

A. Beam commissioning phases

The beam commissioning of the LIGHT prototype has been organized in phases, as mentioned in Sec. IV. From August 2016 to October 2018, as the components were received, the following commissioning phases were performed: (a) PIA with LE test bench, beam up to 40 keV (2016). (b) RFQ with ME test bench, beam up to 5 MeV (2017). (c) SM01 with ME test bench, beam up to 7.5 MeV (2017). (d) SM02 with ME test bench, beam up to 16 MeV (2018). (e) SM03 and SM04 with HE test bench, beam up to 37.5 MeV—shown in Fig. 12 (2018). (f) CM01 and CM02 with HE test bench, beam up to 52 MeV (2018). The different commissioning phases are illustrated in Fig. 13, with details of the accelerated number of protons and maximum beam energies achieved in time.

The commissioning of the LIGHT prototype started at the end of the summer 2016 with the installation and commissioning of the PIA at 40 keV, which was performed with the LE test bench, and the initial results are reported in [9]. The beam commissioning of the RFQ was successfully performed in 2017 and the measurements are reported in [32]. Further measurements from the commissioning of the first modules of SCDTL are reported in [33,34].

During each beam commissioning phase, typical beam measurements included beam intensity, position, profiles, emittances, energy, and energy spread.

Based on these measurements, optimal machine settings were found for the most important machine parameters: (i) electrostatic lens voltages, (ii) horizontal and vertical steerer magnet currents, (iii) rf phase and amplitudes for all the rf modules, (iv) horizontal and vertical positions of the PMQs.

Multiparametric scans were performed with the goal of finding optimal setpoint values for each newly installed equipment.

A considerable effort was put into the implementation of automatic software procedures to perform both (i) automatic calibration of the rf and BD instruments and (ii) scanning of machine parameters synchronized with rf and BD instrument acquisitions. Furthermore, dedicated software tools were developed to simplify and standardize the data analysis and visualization.

Two examples of measurements taken during the beam commissioning are reported in the following and shown in Figs. 14 and 15.

Figure 14 shows the measured horizontal phase space plot of the 5 MeV beam with normalized rms emittance of 0.032 mm mrad (∼0.3 mm mrad total) [32]. The red dots show the sampled phase space area and the 2D density plot shows the beam signal after applying the 5 nA threshold. For this measurement, the slit-slit-FC system was used. Considering the distance between the slits and the resolution of FC electronics, the width of the slit openings was optimized to keep the emittance measurement error below 1%.

Figure 15 reports an example of 2D scan results, where the current of the horizontal steering magnets of MEBT2 was varied while measuring the beam induced signal using a ToF phase probe installed downstream. Such measurements and their analysis helped to optimize the machine parameters and improve the beam performance.

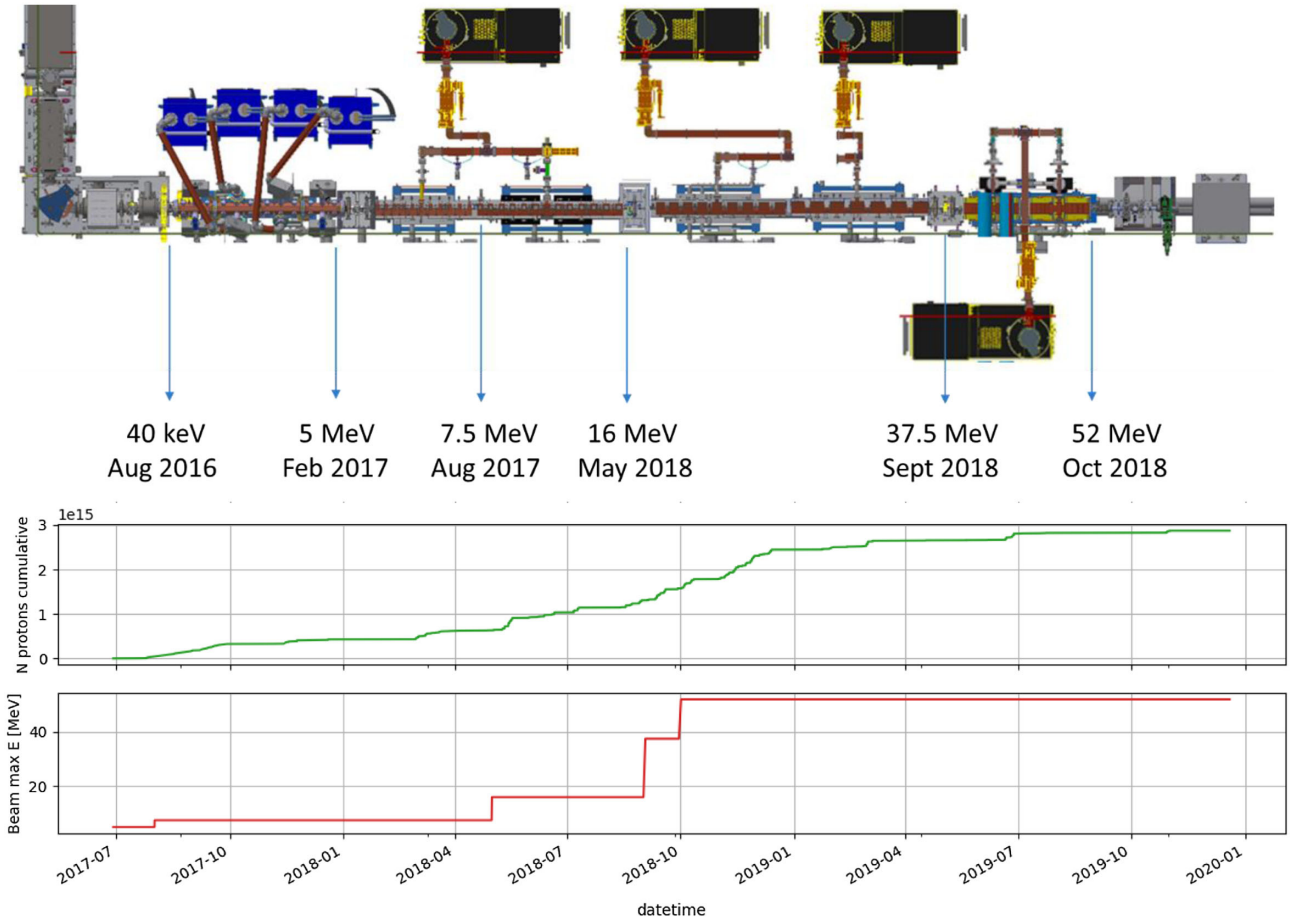

FIG. 13. 3D layout of the LIGHT prototype at different stages of commissioning (top) and evolution in time of the cumulated number of protons accelerated through the linac and maximum beam energy (bottom).

B. Beam measurements at the output of the linac

During the year 2019, beam optimization and beam measurements were performed in the final configuration of the LIGHT prototype. The HE test bench was used for that purpose. The HE test was housing two electromagnet quadrupoles to control the transverse beam size, two BPMs, a ToF system for energy measurements, an optical screen for transverse beam spot size measurements, an FSM for transverse beam profile measurements, and an MLFC for beam energy and charge measurements. The

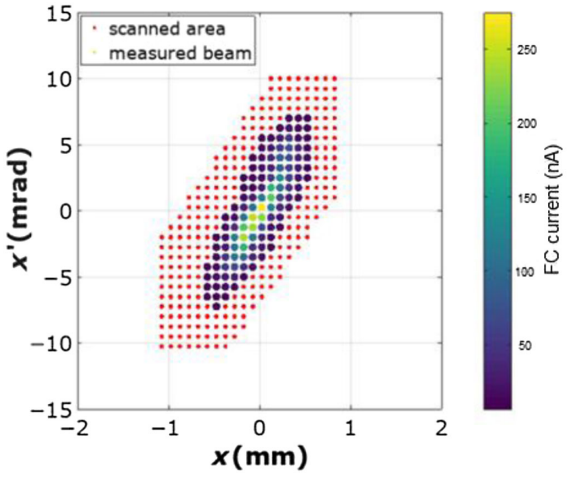

FIG. 14. Horizontal phase space plot of the 5 MeV beam measured with slit-slit-FC system.

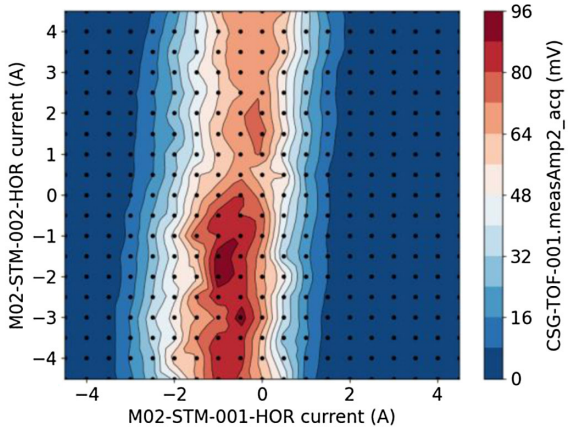

FIG. 15. Example of 2D scans results to find optimal settings of MEBT2 horizontal steerer magnets.

TABLE III. Summary of measured beam characteristics.

Peak Beam current (μA)	8.5 ± 1.5
Beam energy (MeV)	53.27 ± 0.015
Horizontal beam size (mm)	1.73
Vertical beam size (mm)	0.64
Horizontal/vertical rms normalized emittances (mm mrad)	2.186/0.062

electromagnet quadrupoles and FSM were used together for the transverse emittance measurements using quadrupole variation method.

The measured beam characteristics are summarized in Table III and further details are given in the following subsections.

1. Beam energy

The energy of the beam was characterized by ToF and MLFC. Figure 16 shows the energy measured by ToF when the field in CM02 increased gradually (using the moving short). The energy was going up to 53 MeV as the power in the cavity was increasing.

The beam energy and its stability were measured with ToF. The distribution of the beam energy over 1000 pulses when CM02 was set to the maximum power showed an average energy of 53.27 MeV, with a computed standard deviation of 0.015 MeV (Fig. 17).

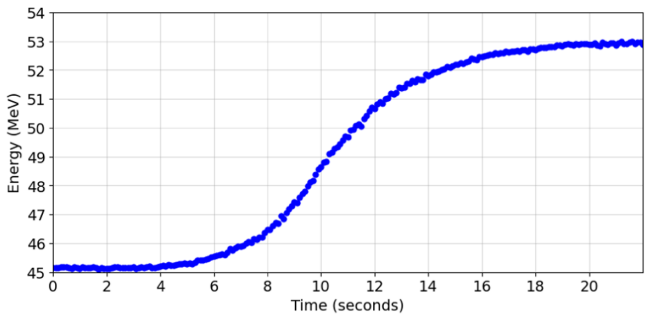

FIG. 16. Energy measured by ToF during ramp-up of CM02.

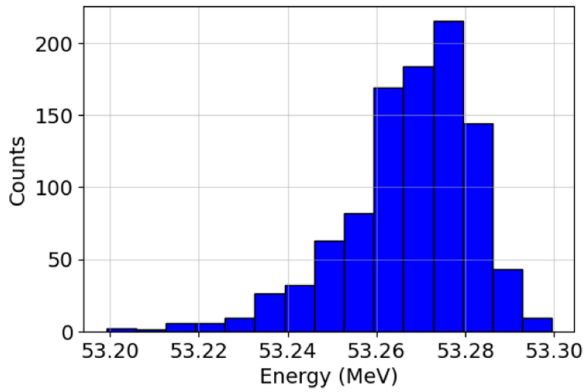

FIG. 17. Distribution of energy measured over 1000 pulses.

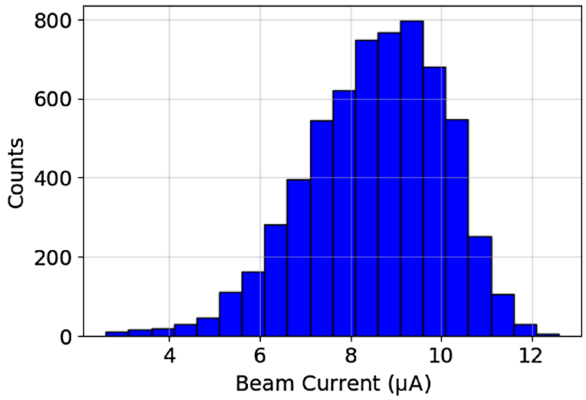

FIG. 18. Measured peak beam current values over 6000 consecutive pulses.

2. Beam current

The beam current and its stability were calculated through the measured charge at MLFC and the beam pulse

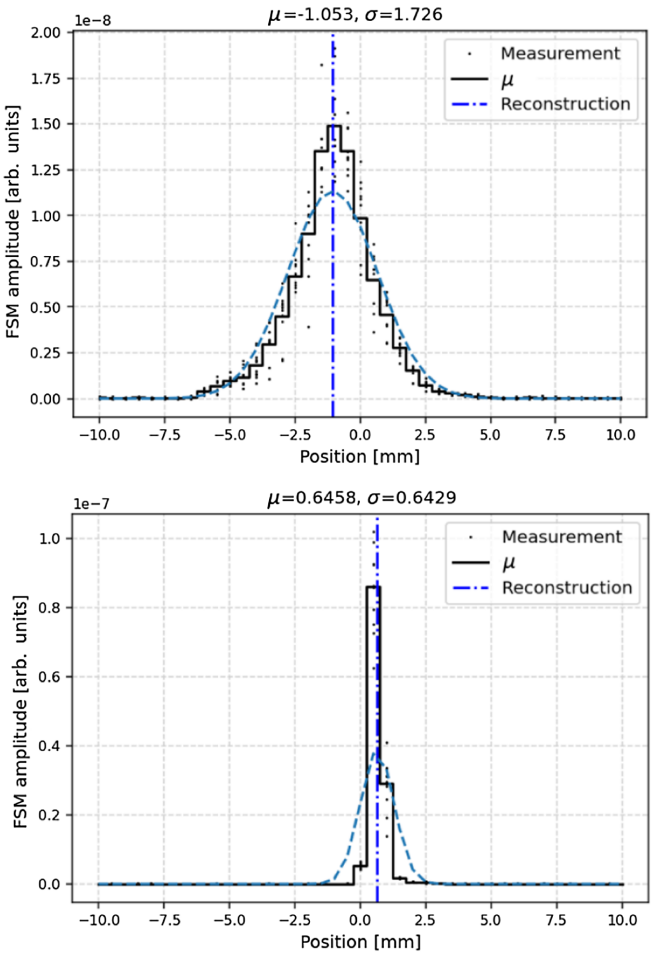

FIG. 19. Horizontal beam profile (top) and vertical beam profile (bottom) measured with FSM. The dots indicated actual measured values per pulse. The black histogram bars are the average values for a given position of the fiber, and the blue dotted line is the reconstructed Gaussian profile.

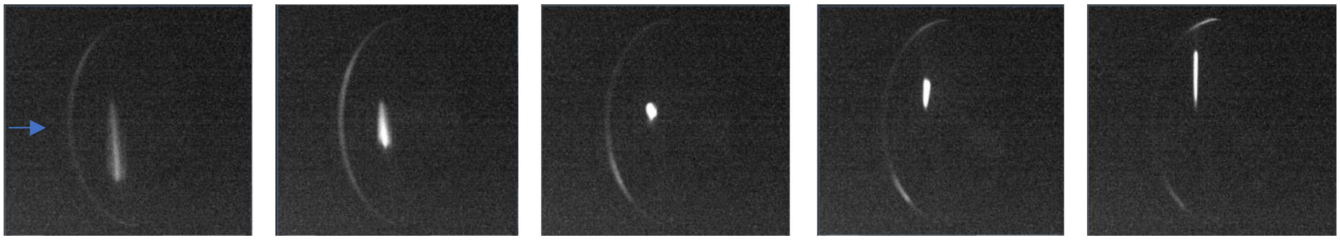

FIG. 20. Beam shape on the scintillating optical screen for different settings of the HE test-bench quadrupoles. The current in the first quadrupole was set at 55 A, while the second quadrupole was scanned in the range of 30 to 50 A in steps of 5 A. The rim of the screen holder is visible on the left side of each figure. The beam direction is indicated by the arrow.

length (0.85 us at the time of the measurement). Figure 18 shows the distribution of measured beam current for 6000 pulses. The average peak beam current is 8.5 μA, with a computed standard deviation of 1.5 μA.

3. Transverse beam profiles and emittances

Measurements of beam profiles were taken using the FSM and with an optical screen.

Figure 19 shows an example of horizontal and vertical beam profiles measured with FSM with settings of the test-bench quadrupole optimized to achieve an extremely narrow beam in the vertical plane. A submillimetric beam size σ_y of 0.64 mm could be achieved at 52.9 MeV.

Figure 20 shows some examples of beam shapes measured with OPT during a quadrupole scan. The beam emittance was reconstructed using a quadrupole variation procedure. The source of the large horizontal emittance value in the measurements reported in Table III was not fully understood. However, as this beam would not fit in the aperture of the CCL modules, it is suspected that it results from an error in the horizontal beam profile measurements.

C. Fast energy and intensity modulation

One of the key features of the LIGHT system is the fast active energy modulation: fast, in the sense of time between energy changes of few ms; active, in the sense that it is achieved by electronics means, without the need for mechanical absorbers. This is made possible by the combination of, on one side, a well-balanced powering of the rf structures (divided into short tanks coupled into modular structures) and, on the other side, a fixed focusing-defocusing (FODO) lattice along the machine made of permanent magnet quadrupoles (PMQs), installed in between the tanks and with a magnetic field gradient chosen such to transport the beam along the linac also even when the rf power is off (see Table I). This feature was demonstrated with the LIGHT prototype during the beam operation run in August 2019.

To validate the energy modulation concept, a database of phase and amplitude settings was uploaded in the LLRF box of CM01 and played in sequence at a high repetition rate. Figure 21 shows the result of the measurement obtained with the noninterceptive ToF system, demonstrating pulse-to-pulse energy modulation. In particular, each point in Fig. 21 represents the measured beam pulse average energy, which was changed electronically every 10 ms (repetition rate of 100 Hz) in order to reproduce (in a loop) a sequence of letters and symbols. The beam could not be accelerated at 200 Hz due to a temporary limitation in the rf power stations. The obtained energy reproducibility of this dataset is in the order of 0.2 MeV.

The other key feature of the LIGHT system, needed for full flexibility in the application of active spot scanning delivery technique, is the fast active beam intensity modulation. This feature was tested in the LEBT section of the

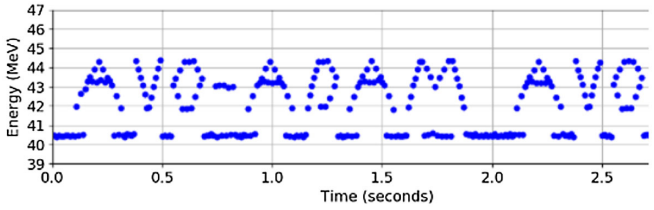

FIG. 21. Example of fast active energy modulation, where the energy of each pulse is adjusted electronically every 10 ms.

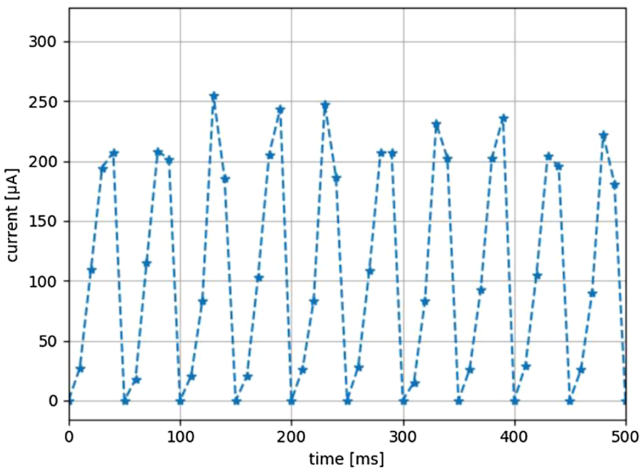

FIG. 22. Example of fast active intensity modulation, measured in the LEBT section of the LIGHT prototype.

LIGHT prototype during the last beam operation run in November 2019.

The LEBT electrostatic elements were used to achieve beam current in the full dynamic range between 0 and 250 μA at a repetition rate of 100 Hz, i.e., changing the beam intensity electronically every 10 ms. Also, in this case, a database of settings was created and used to play a sequence of beam pulses with increasing and decreasing beam intensity. This is shown in Fig. 22, where ten cycles are played in 0.5 s. Further improvements of the system in terms of beam stabilization could not be tested but are expected to allow for fine-tuning of the beam pulse intensity and charge on a pulse-to-pulse basis.

VI. CONCLUSION

The LIGHT prototype represented a significant milestone in the development of high-frequency rf proton accelerators. It was the first to utilize all three types of accelerating structures—RFQ, SCDTL, and CCL—in a single system. This prototype served as a technological feasibility demonstrator for the LIGHT concept and played a crucial role in advancing our understanding of these technologies. It allowed to (i) demonstrate key features of the LIGHT machine, (ii) identify risks and gaps emerging from the integration of the many components and functional subsystems working together, (iii) validate key suppliers, (iv) improve the quality and refine the specifications of several key components, and (v) identify key steps of the installation and commissioning process that can be applied to the first commercial system.

Important lessons learned in the integration of the prototype system included, for example: (i) stability of the rf pulses affected the beam performance. Based on the experience collected by operating multiple modulator and klystron systems, an overall improvement in the specifications was targeted for the first commercial system; (ii) the beam current measurement device (ACT) needed to be protected from the interference from electron dark current generated by the high-frequency rf cavities under high-power operation; (iii) the environmental temperature within the building needed stabilization to improve the beam stability; (iv) optimization in the timing and synchronization setup were identified and implemented for the first commercial system; (v) stability of the beam at the entrance of the RFQ was also analyzed and identified as a source of beam instabilities along the machine; (vi) the rack space, with the proper cable segregation and management, was improved and properly designed for the first commercial system.

All these lessons learned were considered to improve the beam performance in the first LIGHT system.

In addition to its technical achievements, the LIGHT prototype represented a significant example of knowledge transfer and know-how development. This project began as a research endeavor and through the successful demonstration of technological feasibility was able to make the transition into the industrial sector. While there is still room for improvement in beam performance, the LIGHT prototype has successfully demonstrated the integration of a high-frequency linac for proton therapy paving the way for the next phase of technological readiness.

ACKNOWLEDGMENTS

The authors would like to thank Louise Harley-Smeur and Janine Bossé for the careful proofreading of the manuscript. The authors would like to acknowledge the support of all the AVO-ADAM colleagues, and the work done by all external suppliers and collaborators over the years. Furthermore, the authors would like to acknowledge all CERN colleagues for their continuous and crucial support in this work. A special thanks go to the CERN BE and KT divisions.

[1] U. Amaldi, S. Braccini, and P. Puggioni, High frequency linacs for hadrontherapy, in *Reviews of Accelerator Science and Technology, Vol. II (RAST2)* (World Scientific, Singapore, 2009), pp. 111–131, https://doi.org/10.1142/9789814299350_0006.

[2] The IAEA Directory of Radiotherapy Centres (DIRAC), https://dirac.iaea.org.

[3] R. W. Hamm, K. R. Crandall, and J. M. Potter, Preliminary design of a dedicated proton therapy linac, in *Proceedings of the Particle Accelerator Conference, San Francisco, CA, 1991* (IEEE, New York, 1991), https://epaper.kek.jp/p91/PDF/PAC1991_5F2583.PDF.

[4] U. Amaldi, Cyclinacs: Novel fast-cycling accelerators for hadrontherapy, in *Proceedings of the 18th International Conference on Cyclotrons and their applications, Cyclotrons-2007, Giardini Naxos, Italy* (JACoW, Geneva, Switzerland, 2007), https://accelconf.web.cern.ch/c07/PAPERS/166.pdf.

[5] U. Amaldi *et al.*, LIBO—a linac booster for proton therapy: Construction and test of a prototype, Nucl. Instrum. Methods Phys. Res., Sect. A **521**, 512 (2004).

[6] L. Picardi *et al.*, Beam commissioning of the 35 MeV section in an intensity modulated proton linear accelerator for proton therapy, Phys. Rev. Accel. Beams **23**, 020102.

[7] V. G. Vaccaro *et al.*, Design, construction and low power RF tests of the first module of the ACLIP linac, in *Proceedings of the 11th European Particle Accelerator Conference, Genoa, Italy, 2008* (EPSAG, Geneva, 2008), https://accelconf.web.cern.ch/e08/papers/tupp132.pdf.

[8] M. Vretenar *et al.*, A compact high-frequency RFQ for medical applications, in *Proceedings of the 27th Linear Accelerator Conference, LINAC2014, Geneva, Switzerland* (JACoW, Geneva, Switzerland, 2014), https://accelconf.web.cern.ch/LINAC2014/papers/thpp040.pdf.

[9] D. Ungaro *et al.*, LIGHT: A linear accelerator for proton therapy, in *Proceedings of the North American Particle Accelerator Conference, NAPAC2016, Chicago, IL* (JACoW, Geneva, Switzerland, 2016), https://dx.doi.org/10.18429/JACoW-NAPAC2016-FRB1IO02.

[10] V. Khan *et al.*, Simulations and measurements of the CCL modules of the LIGHT accelerator, in *Proceedings of the 9th International Particle Accelerator Conference, IPAC-2018, Vancouver, BC, Canada* (JACoW, Geneva, Switzerland, 2018), https://doi.org/10.18429/JACoW-IPAC2018-MOPML015.
[11] www.pantechnik.com.
[12] www.thalesgroup.com.
[13] M. Vretenar *et al.*, High-frequency compact RFQs for medical and industrial applications, in *Proceedings of the 28th Linear Accelerator Conference, LINAC2016, East Lansing, MI* (JACoW, Geneva, Switzerland, 2016). http://dx.doi.org/10.18429/JACoW-LINAC2016-TH1A06.
[14] B. Koubek, A. Grudiev, and M. Timmins, RF measurements and tuning of the 750 MHz radio frequency quadrupole, Phys. Rev. Accel. Beams **20**, 080102 (2017).
[15] www.tscsrl.net/.
[16] www.vdlgroep.com/en.
[17] www.bjamagnetics.com/.
[18] Toshiba, now Canon: https://etd.canon/en/product/category/microwave/klystron.html.
[19] www.scandinovasystems.com/.
[20] www.jpaw.com.
[21] www.agilent.com/en/product/vacuum-technologies.
[22] www.vatvalve.com/.
[23] R. Moser and H. Pavetits, The LIGHT control and interlock systems, in *Proceedings of the 16th International Conference on Accelerator and Large Experimental Control Systems, ICALEPCS2017, Barcelona, Spain* (JACoW, Geneva, Switzerland, 2017), https://doi.org/10.18429/JACoW-ICALEPCS2017-TUPHA064.
[24] R. Moser *et al.*, Control and interlock systems for the LIGHT prototype, in *Proceedings of the 16th International Conference on Accelerator and Large Experimental Control Systems, ICALEPCS2017, Barcelona, Spain* (JACoW, Geneva, Switzerland, 2017), https://doi.org/10.18429/JACoW-ICALEPCS2017-THPHA130.
[25] www.winccoa.com/.
[26] www.siemens.com/global/en.html.
[27] F. Galizzi *et al.*, A time-of-flight based energy measurement system for the LIGHT Medical Accelerator, in *Proceedings of the 9th International Particle Accelerator Conference, IPAC-2018, Vancouver, BC, Canada* (JACoW, Geneva, Switzerland, 2018), https://doi.org/10.18429/JACoW-IPAC2018-THPML119.
[28] https://leica-geosystems.com/products/laser-tracker-systems#.
[29] A. Temnykh, Vibrating wire field-measuring technique, Nucl. Instrum. Methods Phys. Res., Sect. A **399**, 185 (1997).
[30] S. Benedetti *et al.*, Automatic RF conditioning of S-band cavities for commercial proton therapy linacs, in *Proceedings of the 31st International Linear Accelerator Conference, LINAC2022, Liverpool, UK* (JACoW, Geneva, Switzerland, 2022), https://doi.org/10.18429/JACoW-LINAC2022-MOPOGE06.
[31] A. Jeff *et al.*, A diagnostic test bench for the LIGHT accelerator, in *Proceedings of the 9th International Particle Accelerator Conference, IPAC-2018, Vancouver, BC, Canada* (JACoW, Geneva, Switzerland, 2018), https://doi.org/10.18429/JACoW-IPAC2018-WEPAF001.
[32] V. Dimov *et al.*, Beam commissioning of the 750 MHz proton RFQ for the LIGHT prototype, in *Proceedings of the 9th International Particle Accelerator Conference, IPAC-2018, Vancouver, BC, Canada* (JACoW, Geneva, Switzerland, 2018), https://dx.doi.org/10.18429/JACoW-IPAC2018-TUPAF002.
[33] A. Degiovanni *et al.*, Status of the commissioning of the LIGHT prototype, in *Proceedings of the 9th International Particle Accelerator Conference, IPAC-2018, Vancouver, BC, Canada* (JACoW, Geneva, Switzerland, 2018), https://doi.org/10.18429/JACoW-IPAC2018-MOPML014.
[34] G. De Michele *et al.*, Commissioning status of the LIGHT development machine, in *Proceedings of the 29th Linear Accelerator Conference, LINAC2018, Beijing, China* (JACoW, Geneva, Switzerland, 2018), https://doi.org/10.18429/JACoW-LINAC2018-TUPO013.